Digital Object Identifier 10.1109/TIE.2021.3071683

IEEE Transactions on Industrial Electronics

An MVDC Based Meshed Hybrid Microgrid Enabled Using Smart Transformers

Hrishikesan V M

Chandan Kumar

Marco Liserre

Suggested Citation

H. V M, C. Kumar and M. Liserre, "An MVDC Based Meshed Hybrid Microgrid Enabled Using Smart Transformers," in IEEE Transactions on Industrial Electronics.

An MVDC Based Meshed Hybrid Microgrid Enabled Using Smart Transformers

Hrishikesan V M, *Student Member, IEEE*, Chandan Kumar, *Senior Member, IEEE*, and Marco Liserre, *Fellow, IEEE*

***Abstract*—Decentralized integration of distributed generation (DG) units and loads are increasing in the modern distribution grid. Maintaining the power flow and power quality within their accepted limits is a challenging task. The formation of meshed hybrid microgrids is an effective method to improve the power system. The smart transformer (ST) is a promising solution to establish meshed hybrid microgrids in the distribution system. This paper analyzes the performance of an ST based meshed hybrid microgrid interconnected to the main grid feeder through medium voltage (MV) dc link of a second ST. The coordinated operation of interconnected ST system is proposed to explore the features of the configuration. During normal operation, the MVDC bus voltage is controlled by one ST, and this reduces the complexity of the overall control. The main grid and microgrid MVAC source failure and converter fault conditions are explored to analyze the reliability of the proposed microgrid structure. Moreover, the reactive power support capability and active power losses for the proposed system are compared with the existing solutions. Simulation and experimental results are presented to show the operation of the proposed system.**

***Index Terms*—Meshed hybrid microgrid, medium voltage dc (MVDC) system, smart transformer (ST).**

I. Introduction

THE local consumption of the energy generated from the distributed generation (DG) sources are more economical and it leads to the formation of microgrids [1], [2]. Even though microgrids can exist independent of ac main grid connection, the interconnection with existing ac grids improves the power quality and reliability of microgrids.

In the modern power transmission sector, voltage source converter (VSC) based high voltage (HV) dc transmission systems are popular for the interconnection of DG sources located away from the main grid [3]. The features such as increased power transfer capability and controlled active, reactive power exchange features make this system a better solution in comparison with a conventional ac system [4]. Similarly, in the distribution side, the medium voltage (MV) dc distribution systems are considered to be an emerging trend for integrating the ac microgrids with the main grid [5]–[7]. Some of the features that MVDC distribution system offers are: independent control of active and reactive power flows, improved stability for existing ac distribution system, decoupling grids with different frequencies, etc. [5], [6]. The conventional ac-based microgrids faces challenges in flexibly controlling the active power flow based on the DG output and load condition. Connecting back-to-back (BTB) converter system in a conventional ac distribution line improves the active and reactive power control features in the system and [8] analyzes the voltage sag in a BTB converter connected MV radial ac feeder. Moreover, the reliability of power supply is affected in the conventional configurations and [9] investigates the usage of dc links for providing highly reliable meshed distribution grids.

The ac and dc system interconnections are realized using the power electronic based solutions. The smart transformer (ST) is a power electronics based transformer with energy management features in the distribution system [10], [11]. The ST with three-stage power conversion structure is a suitable candidate for distribution system applications due to the presence of two intermediate dc links at MVDC level and low voltage (LV) dc level [10]. The dc links are appropriate for the integration of battery energy storage system (BESS), electric vehicle (EV) charging station and renewable energy source (RES) [12]. The impact of ST in the MV grid is studied in [13], and the additional features in comparison with conventional power transformer (CPT) are listed. The diverse services that ST offers include frequency regulation [14], peak load shaving operation [15], voltage control [16], capacity enhancement [17], establishing interconnected microgrids [18], hierarchical power management strategy [19], etc.

The meshed hybrid microgrids are considered to be an emerging trend in the reconfiguration of microgrids and the MVDC system is also utilized for the formation of highly reliable meshed grids [7]. The ST's capability to form meshed hybrid microgrid is studied in [20] where the LVDC bus of ST is extended in parallel to the LVAC distribution system, and the DG sources are integrated to the LVDC line. Similarly, the availability of MVDC bus of ST opens up an option to realize the MVDC distribution system [12], [21].

Manuscript received October 29, 2020; revised January 23, 2021; accepted March 26, 2021.

This work was supported by "Visvesvaraya PhD Scheme, MeitY, Govt. of India MEITY-PHD-1228", and research grant ECR/2017/001564, Science and Engineering Research Board (SERB), Department of Science and Technology, India.

Hrishikesan VM, and Chandan Kumar are with Electronics and Electrical Engineering Department, Indian Institute of Technology Guwahati, Guwahati, 781039, India (e-mail: hrishieee@gmail.com; chandank@iitg.ac.in).

Marco Liserre is with Chair of Power electronics, Kiel University, Kiel, D-24143 Germany. (e-mail:ml@tf.uni-kiel.de).

(corresponding author: Chandan Kumar, Ph: +91-361-258-3467, Fax: +91-361-2582542, e-mail: chandank@iitg.ac.in).

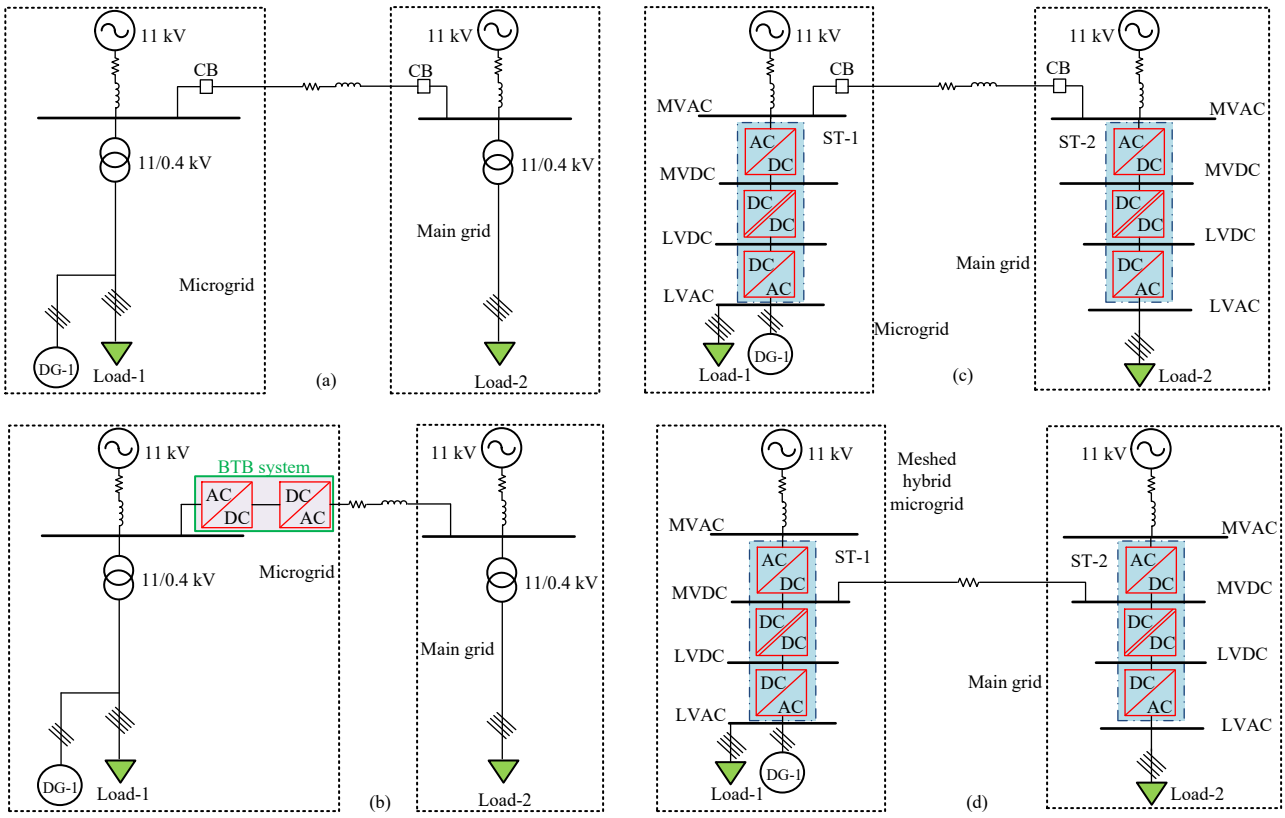

Fig. 1. Single-line diagram of the system. (a) Conventional AC interconnected microgrid [7], [22]. (b) A BTB system interconnected microgrid [8]. (c) The ST based configuration with AC interconnection [21]. (d) Proposed MVDC interconnected meshed hybrid microgrid.

This paper explores the operation of a meshed hybrid microgrid enabled using STs with MVDC interconnection. The features of the proposed structure are compared with the existing solutions, and the various advantages are achieved. The main contributions are summarized as follows:

- The controlled inter grid power transfer during normal operation is presented. In addition, the main grid and microgrid MVAC source and ST MV converter failure conditions are analyzed to investigate the reliability aspects of the proposed system.
- The reactive power capability of the proposed system on the microgrid MVAC bus is studied, and compared with the various existing solutions.
- An analysis is provided to find out the line active power losses in different configurations.
- The operational scenarios are verified with the simulation and experimental results.

The organization of this paper is as follows: system configuration is provided in Section II. Operating modes are described in Section III. Control of power converters is explained in Section IV. Section V provides performance comparison. The simulation results are discussed in Section VI. The experimental analysis is given in Section VII. Section VIII provides the conclusion of the paper.

II. System Configuration

Fig. 1(a) shows a conventional ac microgrid configuration derived from [7], [22]. The 11-kV source in the microgrid is constituted by a number of renewable sources. The microgrid MVAC bus is connected to a feeder in the main grid through AC lines. In the microgrid MVAC bus, the DG unit (DG-1) and loads (Load-1) are connected through 11/0.4 kV CPT. In the main grid MVAC feeder, the loads (Load-2) are connected through a 11/0.4 kV CPT.

Fig. 1(b) shows the modified ac microgrid configuration derived from [8]. For incorporating controlled power transfer, a BTB system connects the microgrid with main grid feeder through AC lines. The loads and DG connections remain same as in Fig. 1(a).

Fig. 1(c) shows an ST based configuration [21]. Both STs use three-stage architecture. The first stage is a three-level, three-phase MV converter connects between MVAC grid and MVDC bus [10]. The second stage consists of a dual active bridge (DAB) converter with high frequency transformer isolation connected between MVDC and LVDC buses [23]. The third stage is a two level, dc-ac converter maintaining three-phase balanced sinusoidal voltage at the LVAC bus of the ST [24]. In the microgrid, the CPT is replaced by ST-1 and the load-1 and DG-1 are connected to the ST-1 LVAC bus. In the main grid MVAC feeder, the CPT is replaced by ST-2 and the load-2 is connected to the LVAC bus. The AC interconnection lines remain same as in the Fig. 1(a). The controlled power transfer capability is absent in this configuration.

In order to incorporate the controlled power transfer flexibility, the Fig. 1(c) is modified. Fig. 1(d) shows the proposed restructured meshed hybrid microgrid using STs. The MVDC

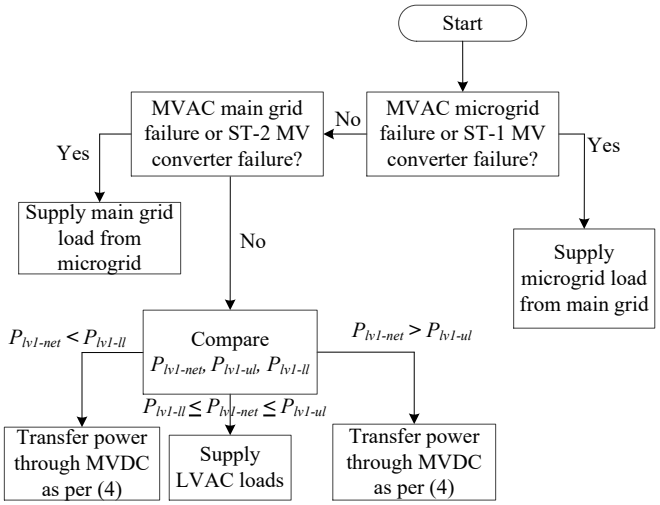

Fig. 2. Flow-chart representation of operation of the meshed hybrid microgrid enabled using STs.

buses of ST-1 and ST-2 are interconnected through MVDC distribution lines. The ST-1 and ST-2 controls the inter grid active power transfer along with the supply of their own loads. The loads and DG connection remain same as shown in Fig. 1(c).

III. Operating Modes

This section discusses the operating modes of the ST based MVDC interconnected meshed hybrid microgrid. Two operating modes are considered in this paper named normal and emergency modes. A flow-chart representation of the operating modes is given in Fig. 2.

A. Normal Mode

The normal operating mode is defined when the following conditions are satisfied:

- microgrid and main grid MVAC sources are operating without any faults and delivering required power
- ST-1 MV and ST-2 MV converters are operating without fault or maintenance.

In the normal operating mode, two scenarios are considered. Independent operation of STs and inter-feeder power transfer. These operations are controlled by the loading on the meshed hybrid microgrid LVAC bus. The net active power loading ($P_{lv1-net}$) is given by,

$$P_{lv1-net} = P_{llv1} - P_{glv1} \tag{1}$$

where P_{llv1} and P_{glv1}, respectively are the active power loading and generation at the meshed hybrid microgrid LVAC bus. The power transfer to the main grid feeder is scheduled only when the ST-1 LVAC net active power loading is less than a predefined active power lower limit (P_{lv1-ll}). Similarly, the active power absorption from main grid feeder is scheduled during microgrid peak load hours when the ST-1 LVAC loading is greater than a predefined active power upper limit (P_{lv1-ul}). The inter-feeder power transfer (P_t) is given by,

$$P_t = P_{opr} - P_{lv1-net} \tag{2}$$

where P_{opr} is the predefined active power operating point. This operating power is defined based on the availability of excess power in the microgrid during low-load condition and amount of load shaving required during peak demand condition. The ST-1 MV converter power reference during this mode of operation is given as,

$$P^*_{stmv1} = \begin{cases} P_{lv1-net}, & \text{if } P_{lv1-ll} \leq P_{lv1-net} \leq P_{lv1-ul} \\ P_{opr}, & \text{otherwise.} \end{cases} \tag{3}$$

The power reference (P^*_{dc}) for MVDC power transfer is given by,

$$P^*_{dc} = \begin{cases} 0, & \text{if } P_{lv1-ll} \leq P_{lv1-net} \leq P_{lv1-ul} \\ P_{opr} - P_{lv1-net}, & \text{otherwise.} \end{cases} \tag{4}$$

During the normal operating mode, the ST-2 MV converter active power reference (P^*_{stmv2}) is given as,

$$P^*_{stmv2} = P_{llv2} \tag{5}$$

where P_{llv2} is the active power loading at the ST-2 LVAC side.

B. Emergency Mode

In the emergency mode, two scenarios are analyzed in this paper. First one is the operation of system during the failure of MVAC microgrid/ST-1 MV converter. Second case shows the failure of MVAC main grid/ST-2 MV converter. In the event of ST-1 MV converter or MVAC microgrid failure, the ST-2 MV converter active power reference is given by (5). The active power exchanged from MVAC microgrid remains at zero and the loads at the ST-1 LVAC bus is served from main grid through MVDC interconnection. Similarly, during the MVAC main grid or ST-2 MV converter failure, the ST-1 supports the ST-2 LVAC loads by the transfer of power through MVDC interconnection.

IV. Power Converter Control

In this section, the control strategy of different power converters are explained for normal and emergency modes. The overall control block diagram is shown in Fig. 3. The subscript i is used to indicate the ST-1, ST-2 related terms ($i = 1, 2$).

The control strategy of ST-1 and ST-2 MV converters are different as they need to control the power transfer between two feeders. ST dc-dc and ST LV converters of ST-1 and ST-2 are controlled in the similar fashion therefore, they are not explained separately.

A. ST-1 MV Converter

In this study, the ST-1 is selected as the primary power controller (PPC) and controls the MVDC power transfer during normal operating mode. During this mode, the active power reference is given by (3). This includes the ST LVAC bus active power and the power transfer requirement. The generalized

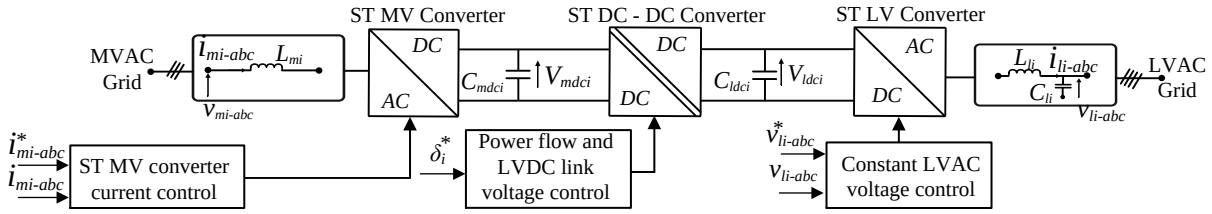

Fig. 3. Overall control diagram of the system.

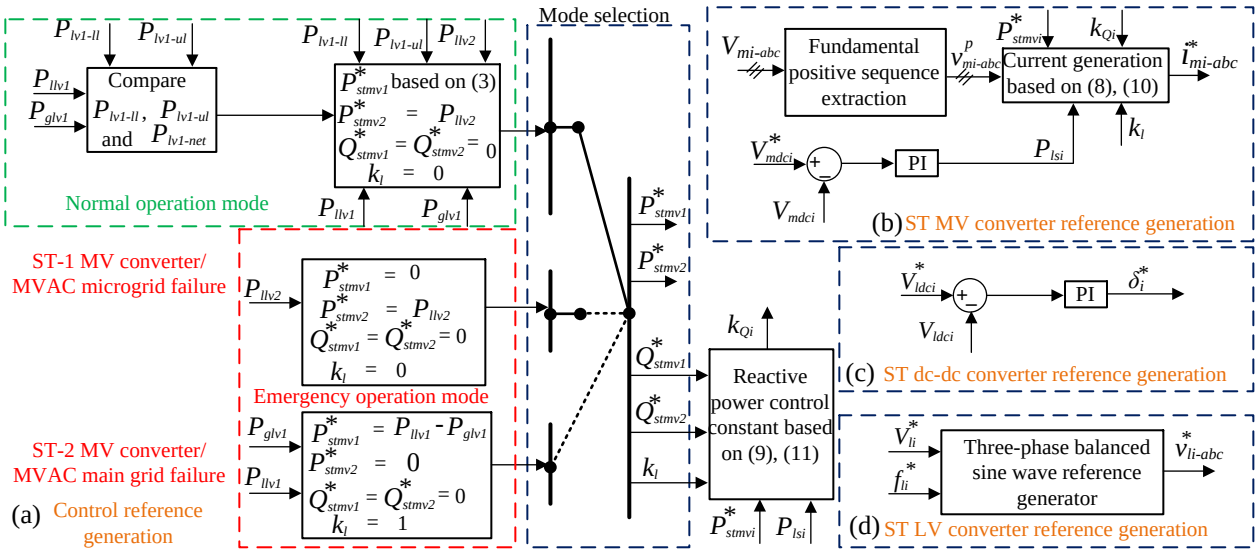

Fig. 4. Reference generation strategy. (a) Control reference generation. (b) ST MV converter current reference generation. (c) ST dc-dc converter reference generation. (d) ST LV converter reference generation.

expression for active and reactive power reference (Q^*_{stmv1}) is written as,

$$P^*_{stmv1} = P_{lv1-net} + K_{tr}P^*_{dc} \; ; \; Q^*_{stmv1} = 0 \qquad (6)$$

where K_{tr} is the control constant for the MVDC active power transfer. K_{tr} is 1 when MVDC active power transfer is activated depending upon the condition explained in Fig. 2 and K_{tr} is 0 when there is no active power transfer.

During emergency mode, when microgrid MVAC grid or ST-1 MV converter failure condition, P^*_{stmv1} = 0. During the MVAC main grid or ST-2 MV converter failure, the P^*_{stmv1} and Q^*_{stmv1} are given as,

$$P^*_{stmv1} = P_{lv1-net} \; ; \; Q^*_{stmv1} = 0. \qquad (7)$$

The ST-1 MV converter use instantaneous symmetrical component theory [25] for the generation of reference currents. The three-phase reference currents (i^*_{m1-abc}) for ST-1 MV converter is given as,

$$i^*_{m1-a} = \frac{v^p_{m1-a} + k_{Q1}(v^p_{m1-b} - v^p_{m1-c})}{(v^p_{m1-a})^2 + (v^p_{m1-b})^2 + (v^p_{m1-c})^2}(P^*_{stmv1} + K_l P_{ls1})$$
$$i^*_{m1-b} = \frac{v^p_{m1-b} + k_{Q1}(v^p_{m1-c} - v^p_{m1-a})}{(v^p_{m1-a})^2 + (v^p_{m1-b})^2 + (v^p_{m1-c})^2}(P^*_{stmv1} + K_l P_{ls1})$$
$$i^*_{m1-c} = \frac{v^p_{m1-c} + k_{Q1}(v^p_{m1-a} - v^p_{m1-b})}{(v^p_{m1-a})^2 + (v^p_{m1-b})^2 + (v^p_{m1-c})^2}(P^*_{stmv1} + K_l P_{ls1}) \qquad (8)$$

where v^p_{m1-abc} are fundamental positive sequence three-phase MVAC bus voltages and P^*_{stmv1} is the reference power depending upon the mode of operation. P_{ls1} is the MVDC bus power loss component generated to maintain the necessary dc bus voltage. The reference (V^*_{mdc1}) and measured (V_{mdc1}) MVDC bus voltages are compared and the error is passed through a proportional integral (PI) controller to generate P_{ls1}. However, for the normal operation, the dc link is controlled by the ST-2 MV converter. The constant K_l = 0 during the entire normal mode of operation. K_l = 1 only when the ST-2 MV converter dc bus voltage control fails due to the ST-2 MV converter or MVAC main grid failure. The constant k_{Q1} controls the reactive power injection to the respective buses and is given by,

$$k_{Q1} = \frac{Q^*_{stmv1}}{\sqrt{3}(P^*_{stmv1} + K_l P_{ls1})}. \qquad (9)$$

The reference currents generated in (8) are used with a PWM controller to generate necessary switching pattern.

B. ST-2 MV Converter

The ST-2 works as a secondary power controller (SPC). During normal operation, the ST-2 MV converter reference active power is given by (5). In addition, during emergency mode of operation with ST-1 MV converter or MVAC microgrid failure, P^*_{stmv2} is also given by (5). When ST-2 MV converter or MVAC main grid fails, P^*_{stmv2} is given as zero. In all conditions, the reactive power exchange (Q^*_{stmv2}) is zero. Similar to the ST-1 MV converter, the three-phase reference currents (i^*_{m2-abc}) for ST-2 MV converter is given as,

$$\begin{aligned} i^*_{m2-a} &= \frac{v^p_{m2-a} + k_{Q2}(v^p_{m2-b} - v^p_{m2-c})}{(v^p_{m2-a})^2 + (v^p_{m2-b})^2 + (v^p_{m2-c})^2}(P^*_{stmv2} + P_{ls2}) \\ i^*_{m2-b} &= \frac{v^p_{m2-b} + k_{Q2}(v^p_{m2-c} - v^p_{m2-a})}{(v^p_{m2-a})^2 + (v^p_{m2-b})^2 + (v^p_{m2-c})^2}(P^*_{stmv2} + P_{ls2}) \\ i^*_{m2-c} &= \frac{v^p_{m2-c} + k_{Q2}(v^p_{m2-a} - v^p_{m2-b})}{(v^p_{m2-a})^2 + (v^p_{m2-b})^2 + (v^p_{m2-c})^2}(P^*_{stmv2} + P_{ls2}) \end{aligned} \tag{10}$$

where v^p_{m2-abc} are fundamental positive sequence three-phase main grid MVAC bus voltages and P^*_{stmv2} is the reference power depending upon the mode of operation. P_{ls2} is the MVDC bus power loss component generated to maintain the nominal dc bus voltage. The reference (V^*_{mdc2}) and measured (V_{mdc2}) MVDC bus voltages are compared and the error is passed through a PI controller to generate P_{ls2}. The PI controller parameters are tuned using symmetrical optimum method [26]. The constant k_{Q2} controls the reactive power injection to the respective buses and is given by,

$$k_{Q2} = \frac{Q^*_{stmv2}}{\sqrt{3}(P^*_{stmv2} + P_{ls2})}. \tag{11}$$

The reference currents generated in (10) are used with a PWM controller to generate necessary switching pattern.

C. ST dc-dc Converter

For both ST-1 and ST-2, the dc-dc converters ensure the constant power flow between MVDC and LVDC buses. This is ensured by maintaining LVDC bus voltage at the constant reference value. The measured LVDC bus voltage (V_{ldci}) is compared with the reference value (V^*_{ldci}). The error is passed through a PI controller to generate a reference phase angle (δ^*_i). This phase angle is maintained between the MVDC and LVDC side converter switching instances. Maintaining this phase shift ensures the required power flow is exchanged between MVDC and LVDC buses [23]. The block-diagram representation is shown in Fig. 4(c).

D. ST LV Converter

A three-phase balanced sinusoidal voltage is required at the ST LVAC bus for both ST-1 and ST-2. The ST LV converter control guarantees the reference value of phase rms voltage (V^*_{li}) is maintained at 50 Hz frequency (f^*_{li}) and 120° phase difference between phases. This is ensured by controlling the ST LV converter as a grid forming voltage source converter [27]. The control block-diagram is shown in Fig. 4(d).

TABLE I
SYSTEM PARAMETERS

System quantities	Values
MV grid voltage	11 kV (L-L)
LVAC voltage	0.4 kV (L-L)
Ac line parameters	1.014 + j1.1929 Ω/km [22], [27]
Load-1, Load-2	0.45 MW, 0.15 MVAr
DG-1	0.2 MVA

TABLE II
PROPOSED RESTRUCTURED SYSTEM PARAMETERS

System quantities	Values
MVDC line parameter	1.014 Ω/km [22]
MVDC voltage	20 kV
ST MV converters	0.55 MVA
ST dc-dc converters	0.45 MW
ST LV converters	0.48 MVA

V. PERFORMANCE COMPARISON

In this section, the performance of the proposed system is compared with different existing solutions [7], [8], [21], [22]. Reactive power capability and active power loss are explained below. Different system parameters considered are given in Table I and Table II.

A. Reactive Power Capability

Reactive power capability of microgrid is an important feature to ensure the necessary voltage support and stability. In the conventional ac microgrid shown in Fig. 1(a), the DG converter can be utilized with full capacity to provide reactive power support. During this time the active power exchange from DG needs to be reduced to zero. The reactive power availability is given as,

$$Q_{DG1} = S_{DG1} \tag{12}$$

where Q_{DG1} is the reactive power rating of DG and S_{DG1} is the rating of DG.

In the second case, the ac system shown in Fig. 1(b) is considered. The reactive power availability (Q_{tot1}) at the MVAC microgrid bus is given by,

$$Q_{tot1} = S_{DG1} + S_{BTB1} \tag{13}$$

where S_{BTB1} is the rating of BTB converter. Here, the DG-1 capacity is also considered for reactive power support.

In the third case, an ST based microgrid is considered without MVDC interconnection as shown in Fig. 1(c). The reactive power availability from ST-1 MV converter is given by,

$$Q_{mv1} = \sqrt{S^2_{mv1-rat} - P^2_{llv1}} \tag{14}$$

where $S_{mv1-rat}$ is the rating of ST-1 MV converter and P_{llv1} is the loading on the LVAC bus.

In the proposed system shown in Fig. 1(d), if the ratings are considered similar to the ST system without MVDC

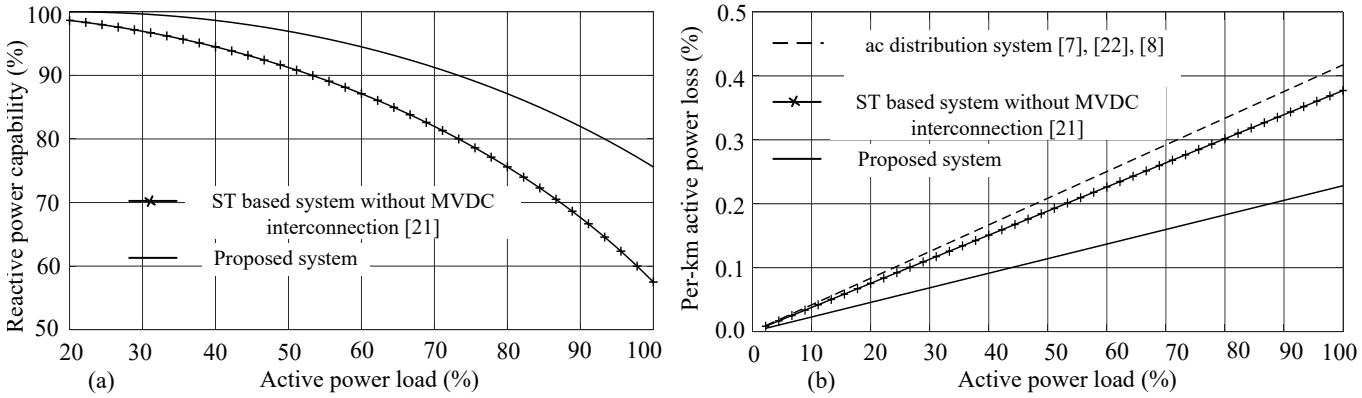

Fig. 5. Performance comparison. (a) Reactive power capability. (b) Active power loss during inter-feeder power transfer.

TABLE III
PERFORMANCE COMPARISON

Parameter	Conventional ac system [7], [22]	Ac system with BTB system [8]	ST based system without MVDC interconnection [21]	Proposed system
Loss during inter-grid power transfer	High	High	Moderate	Low
Controlled inter-grid power transfer	Not available	High flexibility	Not available	High flexibility
Reactive power capability	Low	Low	Moderate	High
Continuous operation of LVAC system during MVAC microgrid failure	Not possible	Limited flexibility	Not possible	Possible
Re-synchronization of DG after MVAC microgrid failure	Required	Required	Required	Not required

TABLE IV
SIMULATION PARAMETERS

System quantities	Values
ST MV converter	L_{mi} = 100 mH
ST LV converter	L_{li} = 0.5 mH, C_{li} = 20 μF
DC link capacitor	C_{mdci} = 2000 μF, C_{ldci} = 2500 μF
ST dc-dc converter	L_{d-d} = 10 mH, f_{sw} = 1 kHz

interconnection, the reactive power availability at the MVAC microgrid is given as,

$$Q_{mv1} = \sqrt{S_{mv1-rat}^2 - (P_{llv1} - P_{dc})^2} \tag{15}$$

where P_{dc} is the transferred power from the main grid feeder.

The percentage reactive power capability ($Q_{cap-perc}$) of ST-1 MV converter is given as,

$$Q_{cap-perc} = \frac{Q_{mv1}}{S_{mv1-rat}} * 100. \tag{16}$$

The reactive power availability in microgrid MVAC bus is constant irrespective of the LVAC loading both in the conventional ac system and ac system with BTB converters. In addition, generally BTB converters are rated for maximum active power transfer. The percentage reactive power capability of ST-1 MV converter is plotted against percentage ST-1 LVAC loading in Fig. 5(a) for the proposed system and the ST based system without MVDC interconnection. The proposed system has better reactive power capability compared to the ST system without MVDC interconnection.

B. Active Power Loss

Active power loss is important during the inter-feeder power transfer. In the conventional ac system shown in Fig. 1(a), the controlled active power transfer is not possible. However, for the system shown in Fig. 1(b), the controlled power transfer is possible with BTB system. The active power loss ($P_{loss-ac}$) for transferring the power from one feeder to other is given by [28],

$$P_{loss-ac} = \frac{P_{li}^2 + Q_{li}^2}{V_{bill}^2} R_{acij} \tag{17}$$

where P_{li} and Q_{li} are the load active and reactive powers of bus-i. V_{bill} is the bus-i voltage (L-L). R_{acij} is the line resistance in Ohms (Ω) per kilometre.

In the ST system without MVDC interconnection shown in Fig. 1(c), the controlled power transfer is not possible since the power is transferred through the ac system. In this case, the ST LV converters supplies the required load reactive power and it is not absorbed from the other feeder. Therefore, the active power loss in this case is,

$$P_{loss-ac} = \frac{P_{li}^2}{V_{bill}^2} R_{acij}. \tag{18}$$

In the proposed ST based MVDC system, the controlled active power transfer is enabled through MVDC interconnection and is written as [28],

$$P_{loss-dc} = \frac{2P_{li}^2}{V_{dci}^2} R_{dcij} \tag{19}$$

where V_{dci} is the MVDC link voltage at the ST-i terminal and R_{dcij} is the line resistance in Ω per kilometre.

The percentage reduction in losses ($\Delta P_{loss-perc}$) for the proposed system as compared to the ST based ac system without MVDC interconnection is given by,

$$\Delta P_{loss-perc} = (1 - \frac{2V_{bill}^2 R_{dcij}}{V_{dci}^2 R_{acij}}) * 100. \tag{20}$$

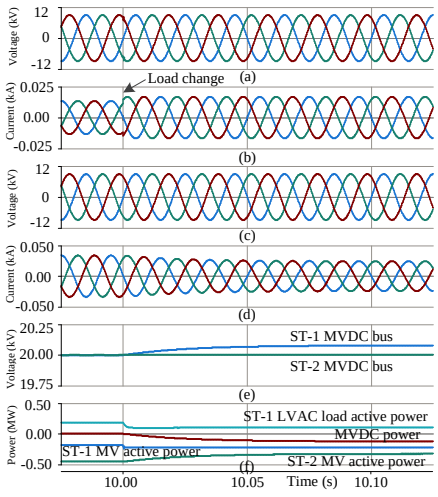

Fig. 6. Simulation results for light-load operation of microgrid. (a) Microgrid MVAC voltages. (b) ST-1 MV converter currents. (c) Main grid feeder MVAC voltages. (d) ST-2 MV converter currents. (e) MVDC bus voltages. (f) Different powers.

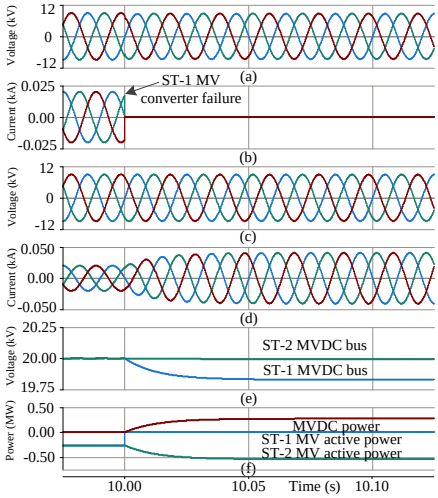

Fig. 7. Simulation results during ST-1 MV converter failure. (a) Microgrid MVAC voltages. (b) ST-1 MV converter currents. (c) Main grid feeder MVAC voltages. (d) ST-2 MV converter currents. (e) MVDC bus voltages. (f) Different powers.

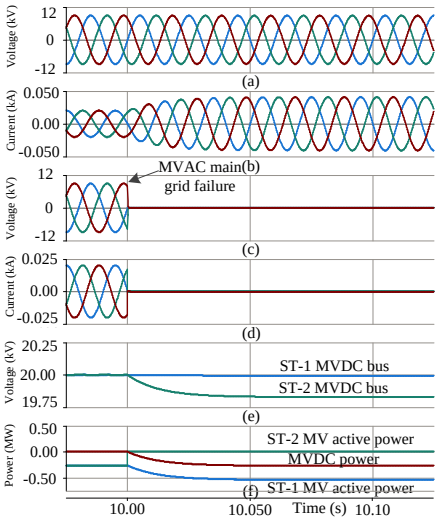

Fig. 8. Simulation results for main grid MVAC source failure. (a) Microgrid MVAC voltages. (b) ST-1 MV converter currents. (c) Main grid feeder MVAC voltages. (d) ST-2 MV converter currents. (e) MVDC bus voltages. (f) Different powers.

Considering same ac and dc resistances, the percentage active power loss reduction is nearly 40% for the proposed system. The percentage of per-kilometre active power loss for a particular amount of active power transfer is calculated. This quantity is plotted against the percentage active power in Fig. 5(b) for different systems and the proposed system curve shows the lowest active power loss percentage.

For the conventional AC configurations or proposed ST based system, the losses are broadly classified as, (1) device losses, and (2) line losses. In this paper, the line loss comparison is given, and the proposed system shows a decrease in losses. Currently, the three-stage ST used in this paper has more device losses than the CPT. However, for the interconnection of remotely located microgrids with the main grid feeder require longer lines, and the line losses will become more significant in the overall losses.

The main features of different distribution systems are compared in Table III. Both the BTB system shown in Fig. 1(b) and the proposed system provides high flexibility in controlled power transfer. The continuous operation during MVAC microgrid failure is possible with short interruption in the BTB based system. The proposed system provides continuous operation without any interruption. After the failure and reconnection of MVAC microgrid, the DG resynchronization is not required in the proposed system. From these characteristics, the proposed system shows an improved performance compared to the other existing solutions.

VI. Simulation Results

The simulation analysis is carried out in PSCAD environment. Normal and emergency mode operations are shown in the simulation. Different parameters are mentioned in Table I, Table II and Table IV.

TABLE V
Experimental Parameters

System quantities	Values
MV grid voltage	150 V
LV grid voltage	110 V
ST MV converters	L_{mv} = 13 mH,
ST LV converters	L_{lv} = 5 mH, C_{lv} = 10 μF
DC link voltage	V_{dc} = 275 V

A. Normal Mode

In Fig. 6 the power transfer during low-load condition of microgrid LVAC bus is demonstrated. The microgrid LVAC bus loading is 40% of the maximum load till t = 10 s. The P_{lv1-ll} is set as 25% of the maximum load. At t = 10 s, the load decreases below P_{lv1-ll}. The P_{opr} is selected as 50% of the maximum load. As discussed in the Fig. 2, the power is transferred from MVAC microgrid to main grid feeder through MVDC line. Fig. 6(a) and (c) show the microgrid and main grid feeder MVAC voltages, respectively. Fig. 6(b) and Fig. 6(d) show the ST-1 MV and ST-2 MV converter currents and ST-2 MV converter currents decreases after load change due to MVDC power transfer from microgrid. The MVDC bus voltages are shown in Fig. 6(e) and ST-1 MVDC link voltage increases to facilitate power transfer. Fig. 6(f) shows ST-1 and ST-2 MV active powers, ST-1 LVAC load active power, and MVDC power transferred.

B. Emergency Mode

In this mode, two cases are analyzed in the simulation, microgrid ST-1 MV converter failure and MVAC main grid source failure. In the first case shown in Fig. 7, the ST-1 MV converter fails due to fault at t = 10 s. Fig. 7(a) shows the MVAC microgrid voltage. Fig. 7(b) shows the ST-1 MV

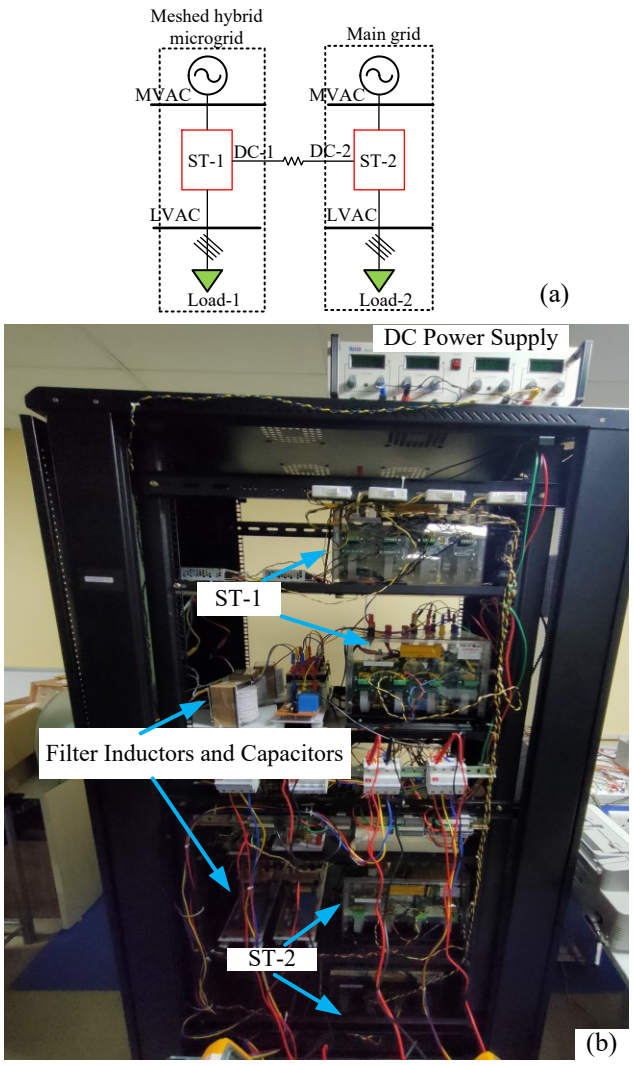

Fig. 9. Experimental setup. (a) Schematic. (b) Photograph.

converter currents which decreases to zero after t = 10 s. Fig. 7(c) shows the main grid feeder MVAC voltages and Fig. 7(d) shows the ST-2 MV converter currents. Fig. 7(e) shows the MVDC bus voltages of ST-1 and ST-2. The ST-1 MVDC bus voltage decreases to facilitate the power transfer. Different active powers are shown in Fig. 7(f).

In the second case, the main grid MVAC source failure situation is analyzed. Till t = 10 s, both the feeders are operating in healthy condition. Fig. 8(a) and (c) show the microgrid and main grid feeder MVAC voltages, respectively. Fig. 8(b) and (d) respectively show ST-1 and ST-2 MV converter currents. Main grid MVAC bus voltages and ST-2 MV converter currents reduces to zero after the main grid source failure. Fig. 8(e) shows MVDC bus voltages and ST-2 voltage reduces after MVAC source failure while ST-1 maintaining MVDC bus voltage at nominal value which facilitates power transfer. Fig. 8(f) shows different powers.

VII. Experimental Analysis

The experimental schematic and photograph is shown in Fig. 9(a) and (b), respectively. The experimental parameters

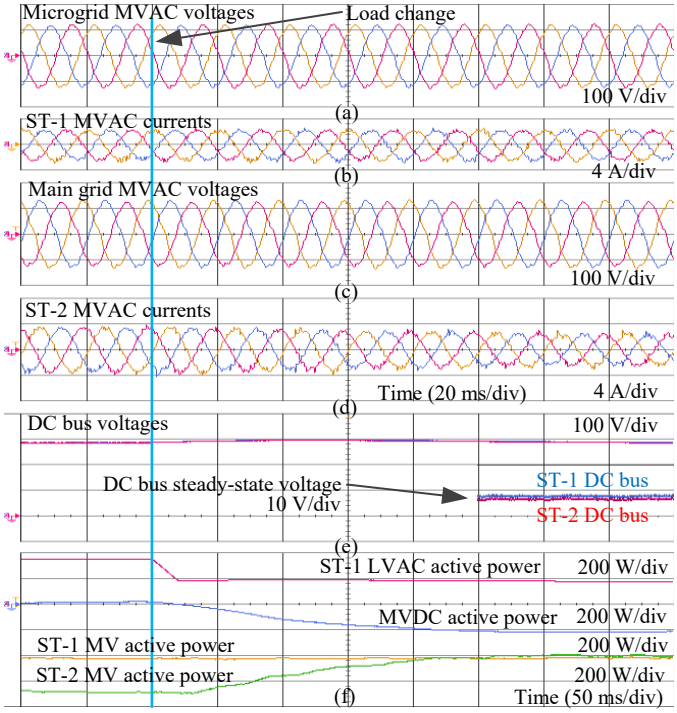

Fig. 10. Experimental results for light-load operation of microgrid. (a) Microgrid MVAC voltages. (b) ST-1 MV converter currents. (c) Main grid feeder MVAC voltages. (d) ST-2 MV converter currents. (e) DC bus voltages. (f) Different powers.

are shown in Table V. All the cases shown in simulation analysis are exhibited in the experimental analysis as well. The normal operation shown in Fig. 10 exhibits the MVDC power transfer based on the loading condition. Till the load change happens, the ST-1 and ST-2 operate by supplying their own LVAC loads. As the load in ST-1 LVAC converter becomes lower than the limit, the active power transfer is initiated and the same is visible in the Fig. 10 waveforms. The ST-2 MVAC currents decreases as seen in Fig. 10(d), since a portion of the ST-2 loads are supplied from microgrid through the MVDC line. Different active powers are shown in Fig. 10(f).

Fig. 11 and Fig. 12 show the operation during emergency condition. In the first case, the ST-1 MV converter fails due to the converter fault and the ST-2 MV converter supplies the ST-1 LVAC loads through the MVDC bus. The dc link voltage of ST-2 remains high to facilitate the transfer. This case is exhibited in waveforms shown in Fig. 11(a)-(f). The Fig. 12(a)-(f) show the MVAC main grid failure condition. In this case, the MVAC grid failure is visible in the voltage waveforms shown in Fig. 12(c) and the microgrid support the ST-2 LVAC load through the MVDC line.

VIII. Conclusion

The presented results verify the performance of MVDC interconnected microgrid configuration enabled with STs. The proposed system provides multiple advantages such as (1) controlled active power transfer capability with high flexibility in power flow directions, (2) for the inter-feeder power transfer, the active power line losses are 40% lower than the ST system

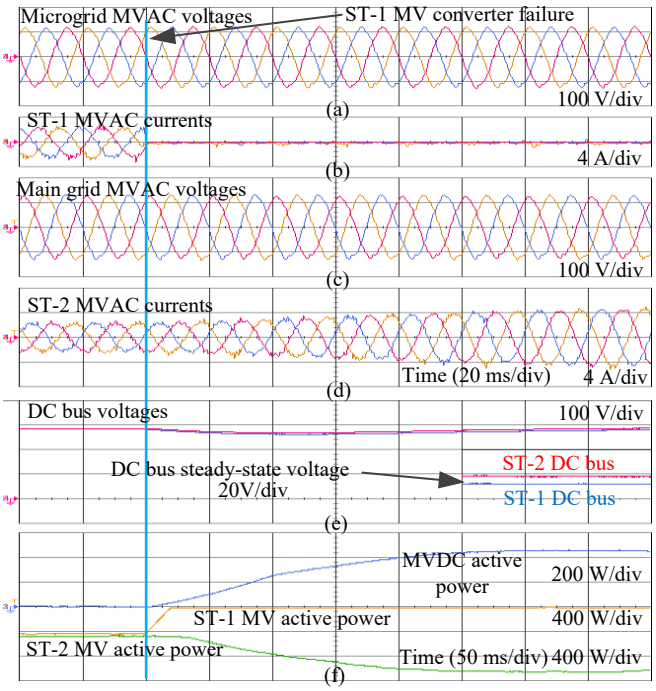

Fig. 11. Experimental results during ST-1 MV converter failure. (a) Microgrid MVAC voltages. (b) ST-1 MV converter currents. (c) Main grid feeder MVAC voltages. (d) ST-2 MV converter currents. (e) DC bus voltages. (f) Different powers.

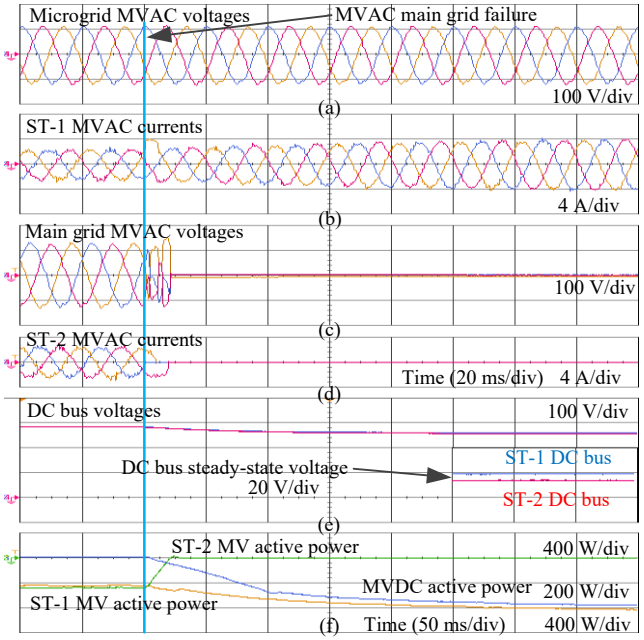

Fig. 12. Experimental results for MVAC main grid failure. (a) Microgrid MVAC voltages. (b) ST-1 MV converter currents. (c) Main grid feeder MVAC voltages. (d) ST-2 MV converter currents. (e) DC bus voltages. (f) Different powers.

without MVDC interconnection, (3) nearly 30% more reactive power capability at full load operating condition in comparison with the ST system without MVDC interconnection, and (4) continuous operation of LVAC distribution system in case of MVAC main grid/microgrid failure conditions and avoids the requirement of DG resynchronization.

REFERENCES

[1] A. Gupta, S. Doolla, and K. Chatterjee, "Hybrid acdc microgrid: Systematic evaluation of control strategies," *IEEE Trans. Smart Grid*, vol. 9, no. 4, pp. 3830–3843, Jul. 2018.

[2] X. Liang, "Emerging power quality challenges due to integration of renewable energy sources," *IEEE Trans. Ind. Appl.*, vol. 53, no. 2, pp. 855–866, Mar. 2017.

[3] T. M. Haileselassie and K. Uhlen, "Impact of dc line voltage drops on power flow of mtdc using droop control," *IEEE Trans. Power Syst.*, vol. 27, no. 3, pp. 1441–1449, Aug. 2012.

[4] Y. Wang, W. Wen, C. Wang, H. Liu, X. Zhan, and X. Xiao, "Adaptive voltage droop method of multiterminal vsc-hvdc systems for dc voltage deviation and power sharing," *IEEE Trans. Power Del.*, vol. 34, no. 1, pp. 169–176, Feb. 2019.

[5] Mvdc plus the grid connector. [Online]. Available: https://new.siemens.com/global/en/products/energy/medium-voltage/solutions/mvdc.html

[6] J. K. Steinke, P. Maibach, G. Ortiz, F. Canales, and P. Steimer, "Mvdc applications and technology," in *PCIM Europe 2019; Int. Exhibition Conf. Power Electron., Intelligent Motion, Renewable Energy Energy Management*, pp. 1–8, May. 2019.

[7] R. Bernacchi, "Mvdc and grid interties : enabling new features in distribution , sub-transmission and industrial networks." [Online]. Available: https://search-ext.abb.com/library/Download.aspx?DocumentID=9AKK107680A0196&LanguageCode=en&DocumentPartId=&Action=Launch

[8] P. Khamphakdi, M. Nitta, M. Hagiwara, and H. Akagi, "Zero-voltage ride-through capability of a transformerless back-to-back system using modular multilevel cascade converters for power distribution systems," *IEEE Trans. Power Electron.*, vol. 31, no. 4, pp. 2730–2741, Apr. 2016.

[9] D. Sciano, A. Raza, R. Salcedo, M. Diaz-Aguilo, R. E. Uosef, D. Czarkowski, and F. de Len, "Evaluation of dc links on dense-load urban distribution networks," *IEEE Trans. Power Del.*, vol. 31, no. 3, pp. 1317–1326, Jun. 2016.

[10] M. Liserre, G. Buticchi, M. Andresen, G. D. Carne, L. F. Costa, and Z. X. Zou, "The smart transformer: Impact on the electric grid and technology challenges," *IEEE Ind. Electron. Mag.*, vol. 10, no. 2, pp. 46–58, Jun. 2016.

[11] S. Bhattacharya, "Transforming the transformer," *IEEE Spectr.*, vol. 54, no. 7, pp. 38–43, Jul. 2017.

[12] F. Ruiz Allende, M. A. Perez, J. R. Espinosa, T. Gajowik, S. Stynski, and M. Malinowski, "Surveying solid-state transformer structures and controls: Providing highly efficient and controllable power flow in distribution grids," *IEEE Ind. Electron. Mag.*, vol. 14, no. 1, pp. 56–70, Mar. 2020.

[13] A. Milczarek and M. Malinowski, "Comparison of classical and smart transformers impact on mv distribution grid," *IEEE Trans. Power Del.*, vol. 35, no. 3, pp. 1339–1347, Jun. 2020.

[14] G. De Carne, G. Buticchi, M. Liserre, and C. Vournas, "Real-time primary frequency regulation using load power control by smart transformers," *IEEE Trans. Smart Grid*, vol. 10, no. 5, pp. 5630–5639, Sep. 2019.

[15] C. Kumar, R. Zhu, G. Buticchi, and M. Liserre, "Sizing and soc management of a smart-transformer-based energy storage system," *IEEE Trans. Ind. Electron.*, vol. 65, no. 8, pp. 6709–6718, Aug. 2018.

[16] X. Gao, F. Sossan, K. Christakou, M. Paolone, and M. Liserre, "Concurrent voltage control and dispatch of active distribution networks by means of smart transformer and storage," *IEEE Trans. Ind. Electron.*, vol. 65, no. 8, pp. 6657–6666, Aug. 2018.

[17] V. M. Hrishikesan, A. K. Deka, and C. Kumar, "Capacity enhancement of a radial distribution grid using smart transformer," *IEEE Access*, vol. 8, pp. 72 411–72 423, 2020.

[18] V. M. Hrishikesan, C. Kumar, and M. Liserre, "Flexible power transfer in smart transformer interconnected microgrids," in *44th Annu. Conf. IEEE Ind. Electron. Soc. (IECON)*, pp. 5535–5540, Oct. 2018.

[19] X. Yu, X. She, X. Ni, and A. Q. Huang, "System integration and hierarchical power management strategy for a solid-state transformer interfaced microgrid system," *IEEE Trans. Power Electron.*, vol. 29, no. 8, pp. 4414–4425, Aug. 2014.

[20] D. Das, V. M. Hrishikesan, C. Kumar, and M. Liserre, "Smart transformer-enabled meshed hybrid distribution grid," *IEEE Trans. Ind. Electron.*, vol. 68, no. 1, pp. 282–292, Jan. 2021.

[21] L. F. Costa, G. D. Carne, G. Buticchi, and M. Liserre, "The smart transformer: A solid-state transformer tailored to provide ancillary services to the distribution grid," *IEEE Power Electron. Mag.*, vol. 4, no. 2, pp. 56–67, Jun. 2017.

[22] R. G. Wandhare and V. Agarwal, "Reactive power capacity enhancement of a pv-grid system to increase pv penetration level in smart grid scenario," *IEEE Trans. Smart Grid*, vol. 5, no. 4, pp. 1845–1854, Jul. 2014.

[23] S. Falcones, R. Ayyanar, and X. Mao, "A dc dc multiport-converter-based solid-state transformer integrating distributed generation and storage," *IEEE Trans. Power Electron.*, vol. 28, no. 5, pp. 2192–2203, May. 2013.

[24] S. A. M. Saleh, C. Richard, X. F. St. Onge, K. M. McDonald, E. Ozkop, L. Chang, and B. Alsayid, "Solid state transformers for distribution systems part i technology and construction," *IEEE Trans. Ind. Appl.*, vol. 55, no. 5, pp. 4524–4535, Sep. 2019.

[25] A. Ghosh and G. Ledwich, *Power quality enhancement using custom power devices*. Springer Science & Business Media, 2012.

[26] R. Teodorescu, M. Liserre, and P. Rodriguez, *Grid converters for photovoltaic and wind power systems*, vol. 29. John Wiley & Sons, 2011.

[27] J. Rocabert, A. Luna, F. Blaabjerg, and P. Rodriguez, "Control of power converters in ac microgrids," *IEEE Trans. Power Electron.*, vol. 27, no. 11, pp. 4734–4749, Nov. 2012.

[28] L. Zhang, J. Liang, W. Tang, G. Li, Y. Cai, and W. Sheng, "Converting ac distribution lines to dc to increase transfer capacities and dg penetration," *IEEE Trans. Smart Grid*, vol. 10, no. 2, pp. 1477–1487, Mar. 2019.

Hrishikesan VM (S'17) received the B.Tech. degree in Electrical and Electronics Engineering from Government Engineering College, Thrissur, India, in 2011 and M.Tech. degree in Power Systems from National Institute of Technology, Trichy, India, in 2014.

He is currently a Research Scholar in the Department of Electronics and Electrical Engineering, Indian Institute of Technology Guwahati, Guwahati, India. His research interests include applications of power electronics in power systems and power quality.

Chandan Kumar (S'13-M'15-SM'19) received the B.Sc. degree from Muzaffarpur Institute of Technology, Muzaffarpur, India, in 2009; the M.Tech. degree from the National Institute of Technology, Trichy, India, in 2011; and the Ph.D. degree from the Indian Institute of Technology Madras, Chennai, India, in 2014, all in electrical engineering.

Since 2015, he is working as Assistant Professor in Electronics and Electrical Engineering department at Indian Institute of Technology Guwahati, India. In 2016-17, he worked as Alexander von Humboldt research fellow at Chair of Power Electronics, University of Kiel, Kiel, Germany. He serves as an Associate Editor of IEEE Access, IEEE Open Journal of Power Electronics, and IEEE Open Journal of the Industrial Electronics Society. His research interests include power electronics application in power system, power quality, and renewable energy.

Marco Liserre (S'00-M'02-SM'07-F'13) received the MSc and PhD degree in Electrical Engineering from the Bari Polytechnic, respectively in 1998 and 2002. He has been Associate Professor at Bari Polytechnic and from 2012 Professor in reliable power electronics at Aalborg University (Denmark). From 2013 he is Full Professor and he holds the Chair of Power Electronics at Kiel University (Germany). He has published 500 technical papers (1/3 of them in international peer-reviewed journals) and a book. These works have received more than 35000 citations. Marco Liserre is listed in ISI Thomson report "The worlds most influential scientific minds" from 2014 and in Clarivate Analytics report "'Highly Cited Researchers" from 2020.

He has been awarded with an ERC Consolidator Grant for the project "The Highly Efficient And Reliable smart Transformer (HEART), a new Heart for the Electric Distribution System".

He is member of IAS, PELS, PES and IES. He has been serving all these societies in different capacities. He has received the IES 2009 Early Career Award, the IES 2011 Anthony J. Hornfeck Service Award, the 2014 Dr. Bimal Bose Energy Systems Award, the 2011 Industrial Electronics Magazine best paper award and the Third Prize paper award by the Industrial Power Converter Committee at ECCE 2012, 2012, 2017 IEEE PELS Sustainable Energy Systems Technical Achievement Award and the 2018 IEEE-IES Mittelmann Achievement Award.